

Impact of MBE-grown (In, Ga)As/GaAs metamorphic buffers on excitonic and optical properties of single quantum dots with single-photon emission tuned to the telecom range

Paweł Wyborski^{1,*}, Michał Gawełczyk², Paweł Podemski¹, Piotr Andrzej Wroński³, Mirosława Pawłyta⁴, Sandeep Gorantla⁵, Fauzia Jabeen⁶, Sven Höfling³, and Grzegorz Sek¹

¹*Department of Experimental Physics, Wrocław University of Science and Technology, Wybrzeże Wyspińskiego 27, 50-370 Wrocław, Poland*

²*Institute of Theoretical Physics, Wrocław University of Science and Technology, Wybrzeże Wyspińskiego 27, 50-370 Wrocław, Poland*

³*Technische Physik, University of Würzburg and Wilhelm-Conrad-Röntgen-Research Center for Complex Material Systems, Am Hubland, D-97074 Würzburg, Germany*

⁴*Materials Research Laboratory, Faculty of Mechanical Engineering, Silesian University of Technology, Konarskiego 18A, 44-100 Gliwice, Poland*

⁵*Lukasiewicz Research Network—PORT Polish Center for Technology Development, ul. Stabłowicka 147, 54-066 Wrocław, Poland*

⁶*Faculty of Engineering and Physical Sciences, University of Southampton, Southampton, SO17 1BJ, United Kingdom*

(Received 29 April 2023; revised 26 August 2023; accepted 30 August 2023; published 4 October 2023)

Tuning GaAs-based quantum emitters to telecom wavelengths makes it possible to use existing mature technology for applications in, e.g., long-haul ultrasecure communication in fiber networks. A promising method redeveloped recently is to use a metamorphic (In, Ga)As buffer that redshifts the emission by reducing strain. However, the impact of such a buffer also causes the simultaneous modification of other quantum dot (QD) properties. Knowledge of these effects is crucial for actual implementations of QD-based nonclassical light sources for quantum communication schemes. Here, we thoroughly study single GaAs-based quantum dots grown by molecular-beam epitaxy on specially designed, digital-alloy (In, Ga)As metamorphic buffers. With a set of structures varying in the buffer indium content and providing quantum dot emission through the telecom spectral range up to 1.6 μm, we analyze the impact of the buffer and its composition on QD structural and optical properties. We identify the mechanisms of quantum dot emission shifts with varying buffer compositions. We also look at charge-trapping processes and compare excitonic properties for different growth conditions with single-dot emission successfully shifted to both the second and third telecom windows.

DOI: 10.1103/PhysRevApplied.20.044009

I. INTRODUCTION

Nonclassical emitters based on semiconductor quantum dots (QDs) fabricated in epitaxial technology have been demonstrated as promising candidates for fundamental components of many nanophotonic devices, including lasers [1–3], optical amplifiers [4,5], and broadband sources [6–8]. Especially in quantum information processing, QDs are also proven to be efficient single-photon sources (SPSs) to realize ultrasecure quantum communication [9–12]. As perhaps the most crucial property

of QD-based structures, emission in the range of highly transmissive second and third telecom windows [9,11,12] has been demonstrated, enabling integration with the existing silica-based optical-fiber infrastructure for the implementation of long-haul telecommunication. Moreover, on-demand QD-based high-purity emission of single, and optionally indistinguishable, photons and the generation of polarization-entangled photon pairs have been shown [13]. Furthermore, many crucial milestones for applying QD devices in secure quantum information technology have been achieved. These include demonstrating advanced nanophotonic devices with high efficiency of single-photon emission [10,14–16], operation at elevated temperatures [12,17,18], integration with a silicon platform [19], and the deterministic fabrication of QD structures [14].

* pawel.wyborski@pwr.edu.pl

The selection of the material system and control of the QD parameters through band-structure engineering, including mismatch of material lattice constants and the resulting strain field, allows the emission energy to be controlled and adjusted to the selected spectral range, particularly second and third telecom windows [20]. The first choice of materials for telecom windows would be InAs QDs grown on InP substrate. They have already been demonstrated as SPSs in this range [11,12,15,21–28], with several implementations of efficient single-photon emitters, additionally generating indistinguishable photons [29–31] and entangled photon pairs (also at elevated temperatures) [27,32,33], and the realization of quantum teleportation [29,33].

InAs/GaAs QDs typically emit below 1200 nm [9,20], and their tuning to the telecom range is more demanding, mainly due to a significantly larger lattice mismatch and built-in strain. But the technology itself has advantages over the InP-based one: it is more mature in some aspects and allows highly reflective distributed Bragg reflectors (DBRs) to be grown; this is more challenging on InP substrates due to lower refractive-index contrast of the lattice-matched semiconductors. Several approaches allow the telecom spectral range to be achieved with GaAs-based structures, like confinement and strain engineering [34–36], modification of the QD composition or QD size increase [37–39], or growing the dots on a metamorphic buffer layer (MBL) made of (In, Ga)As [20,40–45]. However, so far, only the last of these has led to the demonstration of single-photon emission in the third telecom window, which is characterized by the lowest signal attenuation in the fibers [20,41,46]. This solution is promising for applications and allows for easy fabrication of QD emitters inside photonic structures [47,48] and integration with GaAs-based DBRs [20]. In that context, major milestones concern the MOVPE-grown QD systems: emission of polarization-entangled photon pairs [49,50] and indistinguishable photons (also with resonant excitation and in on-demand mode) [51–53], and the implementation of a high-performance photonic structure based on a circular Bragg grating [47,53]. Furthermore, piezo tuning of QD emission energy [54,55] and QD-based coherent control of spin qubits [56] have also been shown. In contrast, for MBE-grown systems, only emission energy shifts towards the telecom range for both laser structures [42,57] and single-QD structures [40,43,45,46,58] have been reported. Therefore, this work attempts to fill this gap by performing a systematic and comprehensive study, because there is still very limited knowledge of the single-dot properties of such GaAs-based telecom-wavelength QDs grown by MBE on an MBL, especially in the wide range of emission energies. Since the QDs grown by MBE can significantly differ from their MOVPE counterparts, they should be carefully investigated to fully verify their potential as nonclassical radiation sources at the telecom range

and exploring them promises to overcome at least some of the limitations encountered and reported for MBL-based QDs grown by MOVPE.

The implementation of efficient SPSs for real applications in secure quantum communication has a few requirements, e.g., high source efficiency, high generation rate and purity of single-photon emission, long coherence of emission, and operation around room temperature (or a simple cooling method). A significant part of these requirements are directly related to single-QD properties [9]. Growing QDs on an MBL, besides the emission-energy change, enables the modification of other application-relevant properties, such as emission polarization, carrier lifetimes and carrier-loss processes, the structure of confined states, and the properties of excitonic complexes like binding energy and fine-structure splitting (FSS). Modifying the strain conditions during growth may change the structural QD parameters (size and indium content) [37] and can also influence the charge environment around the QDs [51], thus affecting all the QD optical properties.

Here, we analyze the structural and optical properties of single (In, Ga)As QDs for several structures with variable indium content in the MBL, resulting in emission wavelengths from 1.1 to 1.6 μm . We use a combination of several complementary spectroscopic techniques, atomic force microscopy (AFM), scanning electron microscopy (SEM), and high-angle annular-dark-field scanning transmission electron microscopy (HAADF STEM), all supported by calculations within the eight-band $\mathbf{k}\cdot\mathbf{p}$ theory to confront the electronic structure with the QD's structural and optical properties, including charge environment and carrier escape paths. We trace all the QD optical parameters for different MBL compositions, indicating the importance of the MBL's influence on QD properties going beyond the simple emission-energy shift. We show that tuning the emission towards the telecom range with increasing MBL In concentration is accompanied by a slight increase of the photoluminescence (PL) linewidth and almost MBL-composition-independent polarization anisotropy of emission. Additionally, we find a slight increase of FSS and a mostly constant value of biexciton binding energy as a function of emission energy. Moreover, we observe changes to the charge environment and their influence on emission properties and PL decay dynamics. Eventually, we show good single-photon emission characteristics in the second and third telecom windows, regardless of the emission shift.

II. METHODS AND MATERIALS

AFM measurements were performed using a commercial Anfatach Level AFM device, offering a spatial resolution of about 2 nm (in plane) and a scanning resolution of about 0.2 nm. An intermittent sample-contact mode was used with a cantilever having a resonance frequency

of about 210 kHz. For SEM, a Hitachi S5000 HRSEM microscope was used, offering electron-beam acceleration of up to 30 kV. Detection of secondary electrons allowed for surface-topography measurements with a maximum resolution of 0.6 nm. Measurements of buried QDs were carried out using HAADF-STEM imaging based on the signals of elastically scattered electrons in the high-angle collection range of 79.5–200 mrad, ensuring the observation of atomic ($\sim Z^2$) contrast in the studied structures. The S/TEM TITAN cube G2 80-300 microscope by Thermo Fisher Scientific was used, equipped with a high-brightness-field emission gun electron source and double-Cs correctors to ensure a spatial resolution of about 70 pm, and operated with an accelerating voltage of 300 kV. Moreover, the super-*X* four-detector x-ray energy-dispersive spectrometer on it allowed us to characterize the composition of the sample. Samples for STEM characterization were prepared using the focused-ion-beam method (employing FEI SEM/XE-PFIB and FEI SEM/GA-FIB microscopes).

Photoluminescence measurements were performed using a standard experimental setup, offering a high-spatial-resolution option based on a microscopic objective (NA = 0.4) focusing the excitation laser and collecting the PL signal with a spatial resolution below 2 μm . A liquid-helium continuous-flow cryostat was used to obtain low temperatures (down to about 5 K) to reduce thermally activated carrier losses and the influence of acoustic phonons on spectral line broadening. It also allowed for temperature-dependent studies. Nonresonant continuous-wave (cw) excitation of the sample was performed with a 640-nm laser line. For quasiresonant excitation and PL excitation (PLE) measurements, a tunable cw laser with a special setup for laser-line filtering was used [59]. Detection based on a 1-m-focal-length spectrometer coupled to a liquid-nitrogen-cooled (In, Ga)As linear array detector with an effective spectral resolution of 20 μeV was used for both PL and PLE. Time-resolved photoluminescence (TRPL) characterization and photon statistics measurements using Hanbury Brown and Twiss configurations in time-correlated single-photon-counting mode were also performed. For this, a 0.32-m-focal-length monochromator for spectral filtering with detection by fiber-coupled NbN superconducting nanowire single-photon detectors, connected to a multichannel picosecond event timer with an overall temporal resolution of the experimental setup of about 80 ps, were used. For pulsed excitation in TRPL, an 805-nm semiconductor diode laser with a pulse-train control possibility (2.5–80 MHz) and approximately 50-ps-long pulses was employed.

Theoretical QD modeling was performed based on available structural data. Initially, a lens-shaped geometry with a height of 5 nm and a base diameter of 40 nm, placed on a 1.2-nm-thick wetting layer, was assumed. A slight 20% in-plane asymmetry was introduced so that the

model was not overly idealized. Initially, a homogeneous material composition was assumed in a QD. Then, Gaussian averaging ($\sigma = 0.9$ nm) of the material distribution was performed to simulate the unavoidable interdiffusion of atoms at interfaces. There were no premises in the structural data for a significant and systematic QD geometry change between the samples. Therefore, constant geometry was kept, and only modification of the composition of the MBL and QDs between the modeled structures was considered. For the dots modeled this way, the strain field within the continuum elasticity theory and the shear-strain-induced piezoelectric field up to the second order in the strain-tensor elements were calculated. The eigenstates of electrons and holes were calculated using an implementation [60] of the $\mathbf{k}\cdot\mathbf{p}$ method [61] that included the effects of strain, piezoelectric field, and spin-orbit coupling. The explicit form of the Hamiltonian used can be found in Ref. [62], and the material parameters are given in Ref. [63] and references therein. Then, states of excitons and higher-order carrier complexes were calculated within the configuration-interaction method with the basis of 32 electron and 32 hole single-particle states. Finally, the optical transition dipole moment and the resulting emission polarization and recombination times [64] were calculated in the dipole approximation [65].

The investigated structures were grown by MBE on GaAs (001) substrate starting with a GaAs buffer layer. Then, a graded-composition (In, Ga)As MBL was grown with different maximal indium contents in the top part to obtain the QD emission redshift. On top of the MBL, InAs material was deposited to form QDs. In the final step, QDs were capped with an (In, Ga)As layer. Due to natural atom-diffusion processes, the obtained QDs are effectively composed of (In, Ga)As. Figure 1(a) presents a layer-structure scheme of the investigated samples, whereas Table I lists all the studied structures, differing in the MBL composition and thickness. More insight into the sample growth can be found in Ref. [40] for structures with indium contents in the top part of the MBL of 0.15, 0.20, 0.24, and 0.29, and in Ref. [46] for the structure with 0.38 indium content. For the In-38% structure, five additional GaAs/AlAs DBR pairs were grown. On top of each structure, a reference (optically inactive) QD layer was grown for structural characterization. For systematic and repeatable characterization of single-QD emission, a combination of electron-beam lithography and wet etching was performed to obtain cylindrically shaped mesas for all structures, except In-38%. For the In-38% structure, circular apertures in a thin silver layer deposited on the sample surface were made, offering similarly repeatable characterization without the necessity for etching, taking advantage of the low spatial (and hence, spectral) density of these QDs [46].

However, one needs to keep in mind that uncapped QDs can differ from buried dots, even significantly [66]. It is known that capping can impact material intermixing,

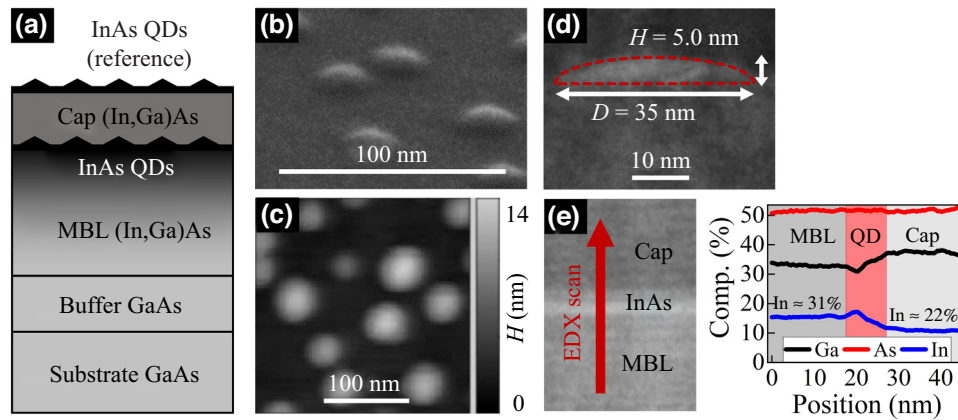


FIG. 1. (a) Scheme of the investigated structure with (In, Ga)As QDs. (b) SEM image of QDs for In-29% structure. (c) AFM image of QDs for In-29% structure. (d) Cross-section HAADF-STEM image of a QD with the In-29% structure. (e) EDX line-scan characterization of the In-29% structure.

additional material accumulation, and cause strain changes. Therefore, the structural properties of the top-layer dots give just an approximate insight into the morphology and density. Nonetheless, one can perform less-demanding characterization by AFM and SEM to get some information. Figures 1(b) and 1(c) present examples of SEM and AFM images of QDs for the In-29% structure. SEM-based results show an average QD height of about 3 nm and a diameter of about 25 nm. AFM characterization of the QD shape shows only slight in-plane asymmetry with an average lateral aspect ratio (η) of about 1.2. High-resolution STEM characterization allowed us to find parameters of buried optically active QDs (width, height, and chemical composition of the QDs and MBL material), which we considered more realistic (but with some other limitations). For the In-29% structure, an exemplary lens-shaped QD cross section is presented in Fig. 1(d). Statistical analysis of many QDs provides average QD parameters: about 5 nm [(4.71 ± 0.25) nm] height (H) and 40 nm [(37.2 ± 2.0) nm] diameter (D). The values are higher than those obtained from SEM characterization, showing the expected influence of the capping layer on the final QD dimensions (and most likely composition). Due to the limitations of the STEM lamellar fabrication accuracy (final QD cross-section location) and the following analysis of images, it is still possible that the size of QDs can be slightly underestimated in this case, mainly for the QD height. The chemical composition distribution inside the dot is also essential, especially for indium with a tendency to segregate, and can significantly modify the QD optical properties. The EDX

spectroscopy characterization accuracy of such a small QD composition is inherently limited. Thus, the indium content inside QDs was obtained by comparing the emission energy with our simulation. However, EDX characterization shows that the indium composition of the MBL and the capping layer (about 2/3 of the top MBL value) is consistent with the optically measured values. Figure 1(e) shows a line scan of the electron beam parallel to the growth direction and crossing the QD layer for the In-29% structure.

III. RESULTS AND DISCUSSION

A. MBL impact on the emission properties of (In, Ga)As QDs

The composition of the top part of the MBL directly impacts the QD emission energy, shifting it to the second (In-29% structure) and third telecom windows (In-38% structure), as shown in Fig. 2(a) from the low-temperature PL spectra for the QD ensemble. This results from the reduced lattice mismatch between the MBL and InAs QD layer, and thus, decreased compressive strain in QDs compared to the pure InAs/GaAs system. Strain reduction directly shifts the QD energy levels. It can also lead to the growth of larger QDs. Both these effects have a direct influence on the emission energy. Another factor directly influencing the confined-state energies is the composition of quantum dots. The increased indium content at the top of the MBL (located directly underneath the QD layer) can favor a higher concentration of indium inside the dots, which also shifts the emission to longer wavelengths. Based on STEM characterization [see Fig. 1(d) for the In-29% structure; it is similar for other samples but not shown here], the average size of QDs does not change significantly when the composition of the MBL is changed, emphasizing the importance of indium-content modification. These observations are consistent with the results of our theoretical calculations, confirming strain modification (driven by the MBL-composition changes) and the

TABLE I. Indium content and measured thickness of the MBL.

| Sample | In content at the top of the MBL (%) | MBL thickness (nm) |
|--------|--------------------------------------|--------------------|
| In-15% | 15 | 780 |
| In-20% | 20 | 960 |
| In-24% | 24 | 1140 |
| In-29% | 29 | 1140 |
| In-38% | 38 | 1200 |

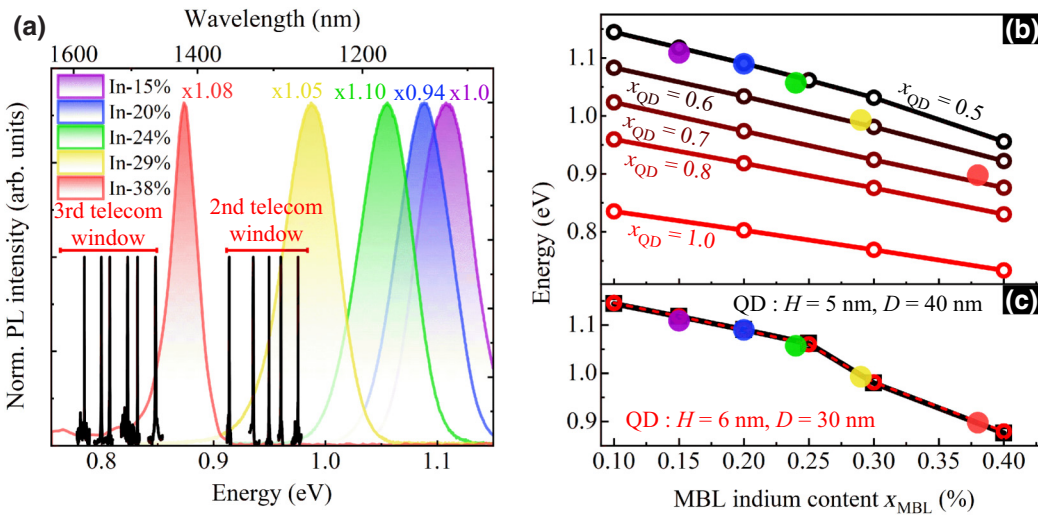


FIG. 2. (a) Normalized PL spectra for the QD ensemble for structures from 15% to 38% indium content in the top part of the MBL (temperature, 10 K; excitation wavelength, 532 nm; cw; multipliers with respect to PL intensity of the In-15% sample) with overlaid single-QD emission lines in the range of second and third telecom windows (temperature, 5 K; excitation wavelength, 640 nm; cw). (b) Calculated QD emission energies as a function of MBL indium content (x_{MBL}) for varying QD indium contents ($x_{\text{QD}} = 0.5, 0.6, 0.7, 0.8, 1.0$) and optically measured emission energies for the investigated structures. (c) Results including QD indium content changes (from 0.50 to 0.65) for two QD geometries: $H = 5 \text{ nm}, D = 40 \text{ nm}$, and $H = 6 \text{ nm}, D = 30 \text{ nm}$ (solid black and dashed red lines, respectively).

indium content inside the QDs as factors that shift the QD emission energy.

Figure 2(b) shows the calculated exciton ground-state energies (lines) together with energies of the PL maxima for the ensemble of dots from Fig. 2(a) (filled symbols) of the examined structures as a function of the In content in the MBL (x_{MBL}). Each line corresponds to changing x_{MBL} only with a fixed geometry and In content inside a QD (x_{QD}). The line for $x_{\text{QD}} = 0.5$ corresponds very well with the first three experimental points. However, the last two points ($x_{\text{MBL}} = 0.29$ and 0.38) do not follow this trend. We assume a higher x_{QD} for $x_{\text{MBL}} > 0.25$ to reproduce this result, with linearly varying x_{QD} from $x_{\text{QD}} = 0.6$ at $x_{\text{MBL}} = 0.3 - 0.7$ at $x_{\text{MBL}} = 0.4$ [see black line in Fig. 2(c)]. The additional red line in Fig. 2(c) presents the results obtained in analogous simulations but for a slightly modified QD geometry: $H = 6 \text{ nm}$, $D = 30 \text{ nm}$, and x_{QD} slightly increased by 0.02 compared to the calculations discussed before. The result almost coincides with the calculations for the nominal values, showing the negligible influence of the QD geometry. These modified dimensions are within the uncertainty limits of determining the QD geometry from structural data but are also justified due to ensemble inhomogeneity. We observe a broadening of the PL peaks of about 50–55 meV for structures In-15%, In-20%, In-24%, and In-29% and approximately 25 meV for In-38%, originating from the distribution of quantum dot parameters (size or dot composition) within an ensemble and typical for InAs QDs [39,67–69], with a possible additional contribution from spatial alloy fluctuations causing local band-gap and strain changes [70].

Figure 2(a) also shows normalized single-QD emission lines within the telecom windows, confirming the possibility of applying these structures in long-distance quantum communication schemes in fiber networks. The possibility of observing individual QDs, even for structures with the highest indium content in the MBL, confirms the good optical quality of our structures. The ensemble emission provides only averaged information about the dots. For applications, especially in nanophotonics and nonclassical light sources for quantum technologies, single QDs are of particular interest. Thus, we focus here on single-QD properties. Figure 3(a) shows the recorded PL linewidths (full width at half maximum, FWHM) for many studied single QDs from samples with different MBL compositions. Error bars in Fig. 3(a) and all subsequent figures correspond to the standard deviation obtained from the fitting procedure. Regardless of the emission energy, we observe relatively large FWHM values significantly above 100 μeV , but comparable to InAs/InP quantum dashes [18,71] and low-strain QDs [72,73]. The linewidths are most likely related to the local electric environment fluctuations (due to discharging and recharging charge traps near QDs), resulting in significant spectral diffusion, i.e., fast fluctuations of QD emission energy broadening the time-integrated spectral lines [74]. This suggests the existence of built-in charge traps in the vicinity of the dots. The median FWHM value changes from 170 μeV for 1.1-eV emission to 300 μeV at 0.8 eV, showing a slight dependence on the MBL composition and indicating an increase in the concentration of defects in the vicinity of QDs with the MBL indium content. Achieving linewidths significantly below 50 μeV ,

comparable to the best results obtained for InAs/GaAs QDs [41,75–77], will require the number of defects near QDs to be reduced by optimizing the growth parameters and MBL composition gradient or by adjusting the composition of the capping layer [45,78]. It is also possible that the interaction of the excitons confined in the dots with charge traps is enhanced for structures with weaker confinement potential, i.e., those with smaller composition differences between the MBL and QDs, that is, high-In-content samples emitting at longer wavelengths. For these, larger in-plane elongation can be expected (see the discussion in the subsection C), which can increase this cross section even further. In addition, surface processing (formation of mesas or aperture structures) can also contribute to the spectral diffusion and inhomogeneous linewidth. Both can provide additional charge traps: (i) for mesas, due to the surface states on the mesa sidewalls, which are in a direct vicinity of some of the dots; (ii) for metallic masks, due to possible charge traps at the semiconductor-metal interface, which, however, are separated from QDs by the cap thickness. Therefore, the impact of mesas is usually a bit more pronounced, especially for smaller mesas (which we have verified for another sample with QDs on the MBL). Please note that we observed linewidths above 70 μeV for all emission lines [Fig. 3(a)], indicating a significant degree of charge fluctuations with a trend to increase for smaller emission energies, both regardless of the type of structure processing (metallic mask or mesa). Thus, broadening must be at least partly (or even predominantly) related to the quality of the MBL.

Polarization of the QD emission for light propagating perpendicularly to the sample surface is mainly defined by the QD in-plane asymmetry through the effects of light- and heavy-hole states mixing and electron-hole exchange interaction. The inequality of oscillator strengths for the orthogonal in-plane axes results in some degree of linear polarization: $\Pi = (I_{\max} - I_{\min})/(I_{\max} + I_{\min})$ [79]. For QDs with significantly decreased strain (like those studied here), asymmetric growth along the [110] and [1–10] crystallographic directions is often observed due to enhanced sensitivity to the atomic steps, and hence, more anisotropic diffusion during the growth of QDs, resulting in the increased Π values [79–82]. For our QDs on the MBL, we observe similar median Π values of 20%–30% for the entire spectral range with a significant spread of values (from near 0% to almost 90%). This is most likely due to some degree of randomness in the orientation of elongation axes in the QD ensemble [79,83]. Figure 3(b) shows the measured Π values for all structures (using a standard fitting procedure [84]). The observed values of Π close to 100% can be related to QDs with a high contribution of light-hole states. Increasing the indium content in the MBL reduces the strain between the base material and the QD layer, which can result in the formation of QDs with increased asymmetry. However, the lack of

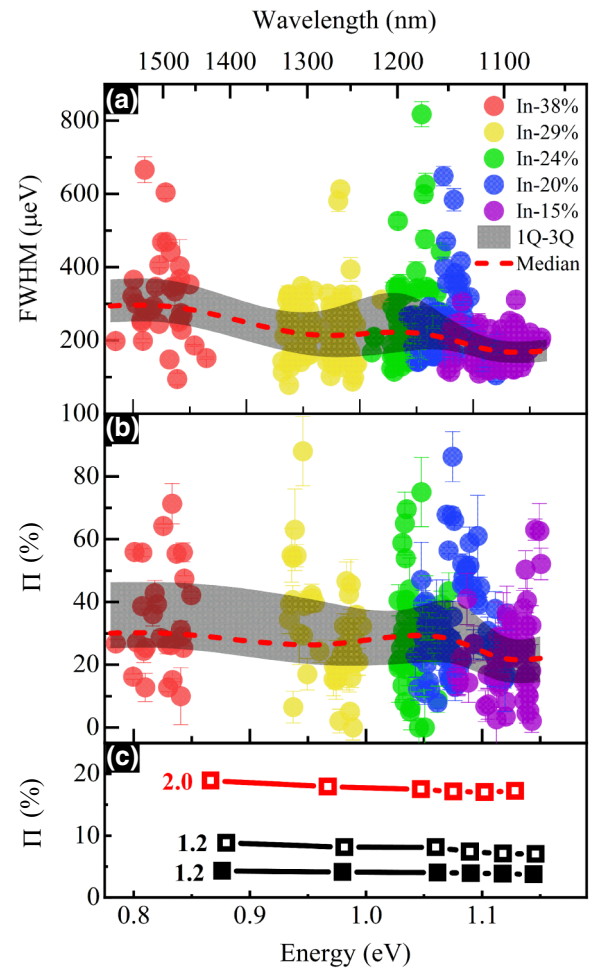


FIG. 3. (a) Linewidth of single-QD emission lines as a function of emission energy for investigated structures from 15% to 38% MBL indium content (marked range between the first and third quartile; red dashed line is the median for individual samples). (b) Π values for single-QD emission lines in a function of emission energy for the investigated structures. (c) Calculated Π values as a function of MBL indium content for various QD parameters: $H = 5 \text{ nm}$, $D = 40 \text{ nm}$ (solid squares), $H = 6 \text{ nm}$, $D = 30 \text{ nm}$ (open squares) with different lateral aspect ratios.

significant Π enhancement for longer wavelengths and our subsequent results for excitonic complexes suggest no substantial changes in the asymmetry of the studied QDs. Based on our calculations, even for QDs with only slight asymmetry ($\eta = 1.2$), a significant mixing of hole states is expected. This is partly due to reduced strain, and hence, decreased splitting of the hole bands. Additionally, particularly for the hole, the reduction in indium-concentration contrast between the top of the MBL and a QD makes the binding potential significantly shallower, leading to stronger wave-function leakage into the interface where the heavy- and light-hole bands cross. This enhancement of hole-subband mixing results in a Π above 7% for a QD

with $H = 6$ nm and $D = 30$ nm [see Fig. 3(c)]. The calculated Π is lower (4%) for a flatter QD with $H = 5$ nm and $D = 40$ nm. This result suggests that the former geometry is closer to the actual dimensions of the investigated QDs. Let us recall that there were no significant differences in the emission energy between both QD geometries [see Fig. 2(c)]. Enhancing the QD asymmetry can further increase the Π value up to 18% for structures with $\eta = 2.0$, as shown in Fig. 3(c). Additionally, the strain in a QD can be overestimated in theory, as it can be additionally relaxed in an actual structure due to some defects located at the top of the MBL. This could explain the underestimation of the Π in our modeling. Overall, the change in the QD emission energy, resulting from modifying the MBL indium content, is not accompanied by a significant change in the Π . We attribute this result to the change in the indium concentration in the dots on In-rich MBLs partly restoring the indium-composition contrast between the top of the MBL and a QD, which tends to decrease for In-rich structures.

B. Quantum dot energy-level structure by photoluminescence excitation

Next, we investigate the QD energy-level structure using photoluminescence excitation spectroscopy. The black line in Fig. 4(a) shows an exemplary emission spectrum for a QD emitting in the third telecom window (In-38% structure). The PLE spectrum for the emission marked with the red arrow is plotted in red. Positions of PLE maxima provide insights into the structures of QD excited states. We also observe agreement between the PL and PLE spectra [green arrow in Fig. 4(a)], which usually

indicates that the same excited state is seen in both the emission and absorptionlike experiments. Knowledge of bright excited QD states enables quasiresonant excitation. By pumping into an excited state, we avoid generating carriers in the barrier and the MBL, significantly decreasing the probability of feeding charge-trap states. This should decrease the PL linewidth for quasiresonant excitation compared to nonresonantly excited PL. In Fig. 4(a), we observe such a reduction in linewidth from $640 \mu\text{eV}$ for nonresonant excitation to $460 \mu\text{eV}$ for quasiresonant excitation (blue line) into one of the QD excited states with an energy of 0.838 eV , as marked with the blue arrow in Fig. 4(a).

The observed linewidth decrease is slight, but still the emission line is relatively broad. It shows that the charge traps expected in the MBL, which are bypassed, at least partly, during the quasiresonant excitation, do not dominate the observed QD linewidths. A lower than expected reduction in PL linewidth may result from built-in excess carriers in the structure (unintentional doping). Another reason may be the formation of charge traps at energies close to the QD emitting states, which are also fed during quasiresonant excitation. For QDs emitting in the third telecom window, we obtain a series of absorption maxima (energies given relative to the QD emission energy). We show these in Fig. 4(b), where we observe a dense structure of higher-energy states with the underlaid simulated levels (blue lines with intensities proportional to the oscillator strength). The measurement range for the excitation-emission energy difference is experimentally limited due to the inability to suppress the excitation laser line at small energy differences (below $\Delta E \approx 15 \text{ meV}$)

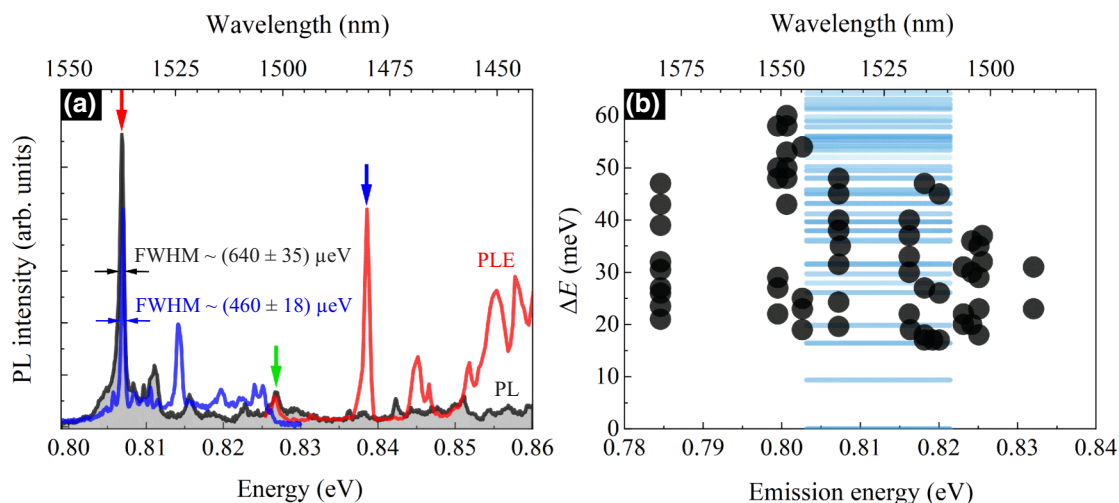


FIG. 4. (a) PL spectrum from a single QD for the In-38% structure for nonresonant excitation (black line). PLE spectrum (red line) for the indicated emission line (red arrow). PL spectra (blue line) based on quasiresonant excitation at the indicated PLE resonance (blue arrow). Observation of a signal for a higher QD state in both PL and PLE spectra (green arrow). (b) Relative energy of excited QD states from single-dot PLE spectra with the underlaid simulated levels (blue lines with intensities proportional to the oscillator strength).

from the emission line. Both experiments and simulations show a similarly dense structure of bright excited states. A dense ladder of excited states is expected in QDs grown in lower-strain conditions provided by the In-rich MBL, making the confinement weaker and the dots relatively large. It also agrees with the observed limited narrowing of the QD emission line for quasiresonant excitation. In the investigated dots, we still excite much higher excited states than in typical InAs/GaAs QDs where the energy ladder is sparser.

C. Excitonic complexes

As the QD emission is directly defined by the excitonic complexes it confines, we look in more detail at their properties. We characterize exciton and biexciton complexes in all investigated structures with high-spatial-resolution PL measurements. Figure 5(a) shows exemplary spectra of the excitation-power dependence of exciton (X) and biexciton (XX) radiative recombination in a single QD emitting in the third telecom window (structure In-38%). We identify the emission lines based on their power-dependent intensities, which are linear for the exciton and almost quadratic for the biexciton [Fig. 5(b)] [85]. Additionally, we confirm their origin in the antiphase dependence of the energy position as a function of the linear polarization angle [Fig. 5(c)] [86].

By fitting to the low-excitation-power part of the dependences, we find exponents of 1.01 ± 0.04 for the exciton and 1.68 ± 0.11 for the biexciton. We find no clear dependence between the exponents and emission energy based on all investigated X - XX pairs. The average exponent for X is 0.948 ± 0.031 and 1.755 ± 0.050 for XX . Their ratio

is about 1.85, i.e., it does not reach the typical value of 2 expected for QDs in the strong-confinement regime [85], suggesting an intermediate-confinement regime, which is expected given the dense ladder of hole states with level separations lower than the electron-hole Coulomb interaction of about 15 meV.

The biexciton binding energy, determined from the energy separation between the X and XX lines, for the discussed pair is about 2.2 meV. Figure 6(a) shows the values of the biexciton binding energy for all examined X - XX pairs. We observe a slight change with the emission energy (reduction of the binding energy for longer wavelengths). The range of values within a QD ensemble is relatively broad (over 1.5 meV in the most-dispersed case), whereas the changes between different structures are less pronounced. This confirms the very weak dependence of XX binding energy on the MBL composition. The obtained XX binding energies, ranging from 1.06 to 2.94 meV, are comparable to those for standard GaAs-based QDs [87,88] and those grown on the MBL by other groups [37,89]. We compare the experimental values with simulations for QDs ($H = 6$ nm, $D = 30$ nm) with different η . We show this in Fig. 6(a), where good agreement may be seen.

Based on the polarization dependence of X and XX energies [Fig. 5(c)], we determine a FSS of (50 ± 5) μeV for the selected case, suggesting at least some QD-confinement potential asymmetry. All the collected FSS values are presented in Fig. 6(b). They range from 5 to 64 μeV, with some tendency toward higher FSS for longer wavelengths; however, their accuracy is limited by relatively large inhomogeneous linewidths. The observed weak trend may indicate an increase in the asymmetry of the dots grown under lower-strain conditions (higher

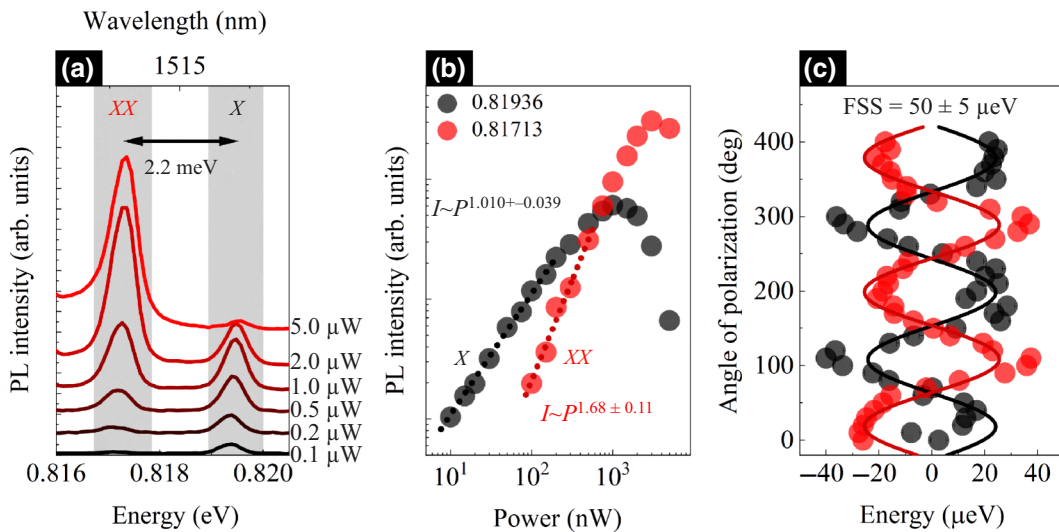


FIG. 5. (a) PL spectra from a single QD for nonresonant excitation (sample In-38%) for excitation power values from 0.1 to 5 μW. (b) Intensity of exciton (X) and biexciton (XX) lines as a function of excitation power with power-function fits (lines). (c) Emission energy of X and XX lines for different linear polarization angles with sine fits (lines).

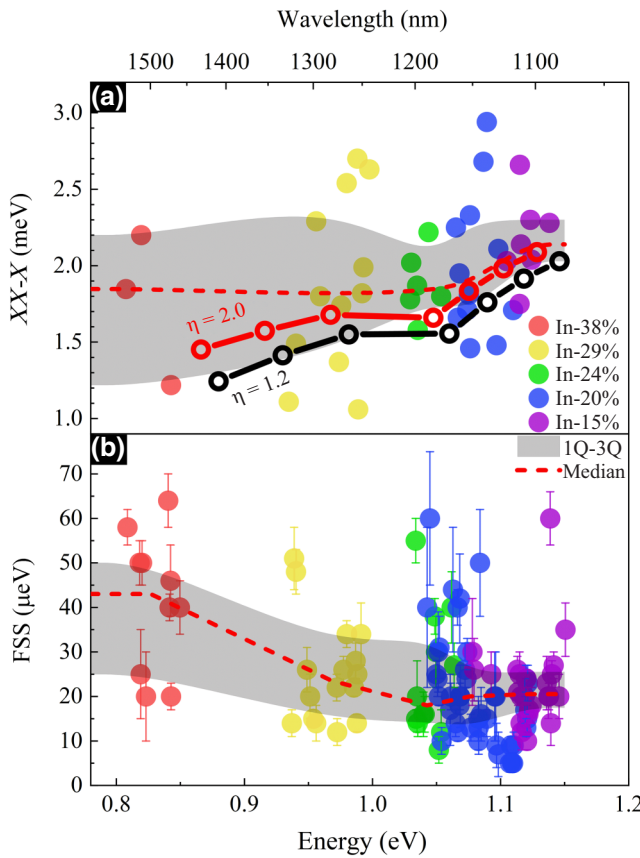


FIG. 6. (a) XX binding energies (solid points) as a function of emission energy with a marked range between the first and third quartiles; dashed red line is the median for individual samples. Theoretical simulations of binding energies for QDs ($H = 6$ nm, $D = 30$ nm) with different η (open points). (b) Fine-structure splitting of single-QD emission lines as a function of emission energy (marked range between first and third quartiles; dashed red line is the median for individual samples).

indium content in the MBL). Such increased asymmetry could, in turn, be connected to the high Π observed for many lines with a slight increase in the redshift of emission. However, in our case, the FSS trend is barely noticeable and the obtained values are relatively low over the entire spectral range (especially for wavelengths below 1350 nm), which usually corresponds to rather in-plane symmetric nanostructures or symmetric confinement potential for at least one of the carriers. In addition, in Fig. 6(b), we do not include cases with almost zero FSS. These would be difficult to distinguish from the charged-exciton-emission lines in polarization-resolved analysis, considering the finite spectral resolution of our setup of about 20 μeV, and the limitations of the analysis of the results (about 5 μeV in the fitting procedure and line separation). Therefore, the actual FSS values (especially for shorter wavelengths) can be even lower.

D. Carrier dynamics

The PL decay time of QD emission is primarily related to the radiative lifetime of the confined carriers, especially at sufficiently low temperatures, when the contribution from nonradiative processes is minimized. The radiative lifetime directly corresponds to the oscillator strength of optical transitions, related to the confinement potential in a QD. It is crucial for implementing single-photon sources based on QDs, as it impacts the maximal frequency of operation of such devices. Our QDs are characterized by either fast monoexponential decays or a combination of short and long decay times, as shown in Figs. 7(a) and 7(b), respectively, with exemplary results showing the fast and slow decay components.

The mean values of the measured decay times (nonresonant pulsed excitation) for many investigated lines (different complexes; uncategorized) and identified exciton and biexciton complexes are presented in Table II. In most cases, two decay times are observed, especially for QDs emitting above 1200 nm, which may indicate the presence of other processes manifested by a slow decay component for structures with increased indium content in the top part of the MBL. They may be related to the influence of the local QD charge environment, i.e., additional energy states likely associated with neighboring charge-trapping defects from which a delayed refilling of QDs can occur. The concentration of such charge traps in the MBL can be elevated for higher indium contents. This agrees with the observed linewidth increase for QDs emitting at longer wavelengths, as discussed above. The increased influence of defect states can also result in the observation of the additional decay time. Two decay times have been seen for analogous QD

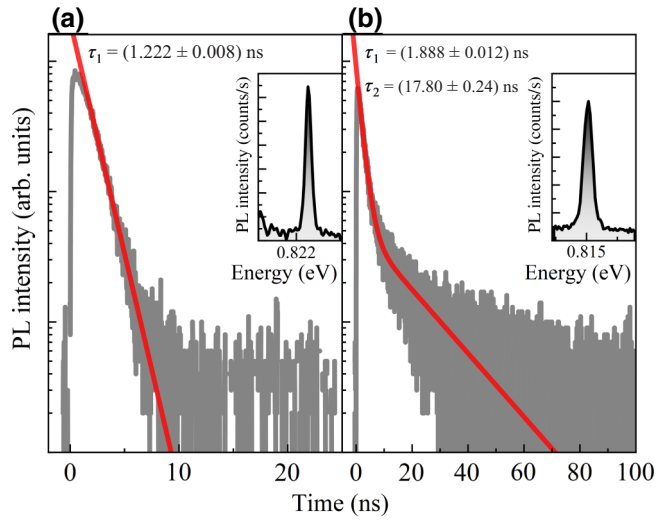


FIG. 7. TRPL results for (a) fast single-exponential decay and (b) combination of short and long decay times with additional exponential fitting (red line) for a single QD (structure In-38%) nonresonantly excited.

TABLE II. Decay times of single-QD emission lines (mean values) for all investigated structures divided into the spectral ranges of emission. τ_1 (short) and τ_2 (long) cover many QD lines of different complexes, while τ_X and τ_{XX} are the short decay times for identified X and XX lines only.

| | <1200 nm | 1200–1400 nm | 1400–1600 nm |
|--------------------|-----------------|-------------------|-----------------|
| τ_1 (ns) | 1.15 ± 0.16 | 1.432 ± 0.081 | 1.52 ± 0.48 |
| τ_2 (ns) | Not observed | 5.20 ± 0.68 | 6.4 ± 1.3 |
| τ_X (ns) | 1.56 ± 0.35 | 2.26 ± 0.40 | 2.64 ± 0.43 |
| τ_{XX} (ns) | 0.81 ± 0.15 | 1.10 ± 0.20 | 1.39 ± 0.12 |
| τ_X/τ_{XX} | 1.86–2.00 | 1.81–2.45 | 1.73–2.04 |

structures emitting in the third telecom window and fabricated by MOVPE, confirming a similar impact of the charge traps in the MBL [51].

We observe a slight increase in the short decay times (for the uncategorized QD lines of different complexes) for longer wavelengths, from an average of 1.15 ns for QDs emitting below 1200 nm to 1.52 ns for QDs emitting in the third telecom window (1450–1600 nm). This change suggests a lower oscillator strength for In-rich MBL dots. Comparable trends were observed for the identified X and XX complexes (see Table II). Information on their lifetimes is relevant due to excluding other complexes from the decay-time statistics. We find an average exciton lifetime of 1.56 ns for QDs emitting below 1200 nm and 2.64 ns for dots in the third telecom window. These times are slightly longer than those typically observed in InAs QDs emitting below 1000 nm [9] and for similar structures grown by MOVPE [41]. Similarly, we observe increased X and XX decay times for longer wavelengths. It is worth noting that, for the identified X and XX emissions, a slow decay component is also present for most of the lines. Table II also presents the exciton-to-biexciton lifetime ratio, which is often used to identify the QD exciton-confinement regime. We observe τ_X/τ_{XX} ratios around 1.8, i.e., below 2 for all the spectral ranges and all MBL compositions, suggesting intermediate confinement. This agrees with a dense-confined-state ladder, especially for holes. For QDs emitting in the second (third) telecom window, the separation is about 21 meV (\sim 15 meV) for electron states and about 4.3 meV (\sim 3.8 meV) for hole states (for a QD with $H = 6$ nm and $D = 30$ nm, $\eta = 1.2$). The separation of single-particle states compared to the exciton binding energy of about 12–15 meV confirms a weaker confinement potential and is characteristic of the intermediate-confinement regime.

E. Single-photon emission in the telecom range

From the photon autocorrelation measurements for the exciton emission, we obtain the second-order correlation functions, $g^{(2)}(\tau)$, under nonresonant cw excitation

(640 nm), which give an insight into the quality of single-photon generation. Figures 8(a) and 8(b) show exemplary results in the second and third telecom windows.

For most of the investigated cases, the as-measured values of $g^{(2)}(0)$ are below 0.2, demonstrating the telecom-range single-photon emission from our QDs with good source purity, regardless of the spectral range and modifications in the MBL [Fig. 8(c)]. Fitting the experimental data [46] provides even lower values, as marked by rimmed symbols in Fig. 8(c). The determined $g^{(2)}(0)$ values are comparable with those for InAs/InP and InAs/(In, Ga, Al)As/InP QDs (both symmetric and asymmetric) obtained under nonresonant excitation [15,21,28, 90–92], but are still worse than the best reported values for other GaAs-based dots [12,20]. The level of signal detected from the investigated QDs is still not very high (below 5000 counts/s for the best cases at saturation using single-photon detectors), which results in limited accuracy of $g^{(2)}(0)$ determination; this can be a limitation in the precise derivation of very low $g^{(2)}(0)$ values. It can be improved when the material's structural quality is improved, and hence, the contribution from nonradiative losses decreases.

The $g^{(2)}$ measurements under pulsed excitation allow us to demonstrate single-photon-triggered QD emission in both the second and third telecom windows, as shown in Figs. 9(a) and 9(b). The limitation of these experiments was a relatively weak signal under these conditions, which forced us to use higher excitation when compared to cw measurements, plus the existence of the long-decay-time component in PL. As a consequence of the latter, the counts in between the pulses do not reach the zero level (or the detector dark-count level), which is even more severe for the 1.5- μ m (In-38%) case. Therefore, we used a 2 times smaller excitation repetition [see Fig. 9(a)]. The near-saturation excitation conditions do not allow us to directly connect the fitted decay times to the result of dynamics characterization obtained for much lower average powers. Independently of these, we observe a significant signal reduction for the zero time delay, indicating clear single-photon emission in a triggered mode. The nonideal suppression of multiphoton events for small delays [see corresponding magnification of $g^{(2)}(\tau)$ in Figs. 9(c) and 9(d)] is additionally hindered by observation of the typical fingerprint of the carrier-recapture processes from the charge states surrounding the dots [16,93,94]. To account for the long-decay-time component, two decay times were included in the fitting formula [95]; however, this was insufficient to reconstruct the near-zero delay range properly, where the inclusion of recapturing was necessary (after Ref. [16]). Based on the fitting with this dependence, we obtain $g^{(2)}(0)$ values of 0.07 and 0.17 for the 1.3- and 1.5- μ m cases, respectively, and the natural $g^{(2)}(\tau)$ background on a similar level of about 0.05–0.1, estimated to be the detector dark counts. Despite the mentioned

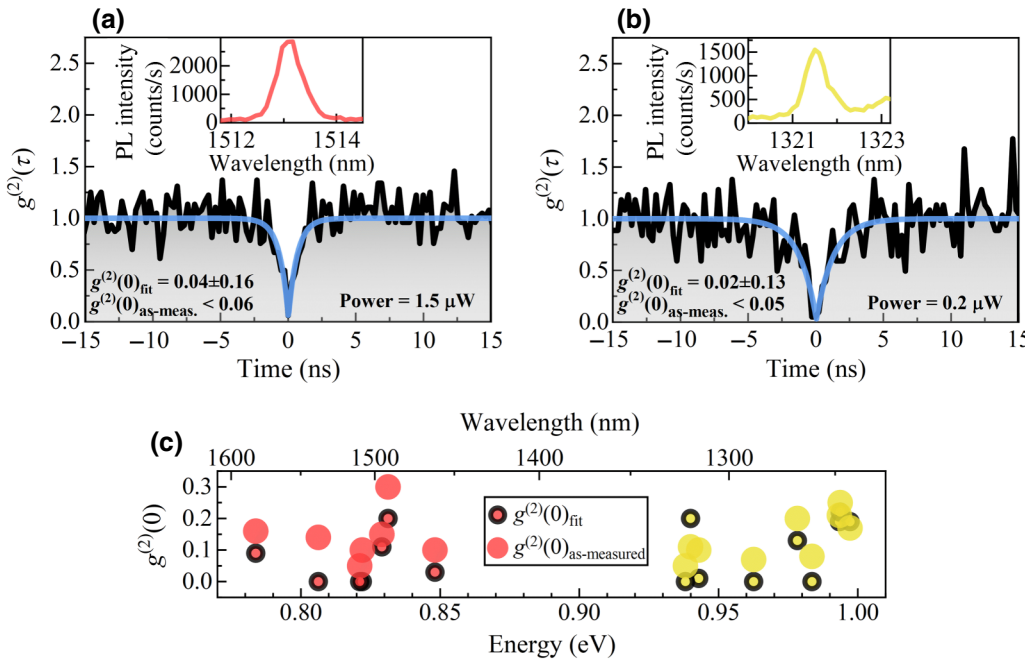


FIG. 8. Second-order correlation function, $g^{(2)}(\tau)$, for X emission under cw excitation with the 640-nm line (a) for structure In-38% and (b) for structure In-29%. Blue line is the fit to experimental data, and insets show the emission spectra of the investigated lines. (c) Values for all investigated cases from both structures.

limitations, this single-photon-emission purity indicates the application potential of these QDs, where an improvement in the characteristics should be possible with resonant excitation and further optimizations in the growth procedure. Optimization of MBL growth parameters, as well

as the capping layer, should allow the number of defects in the structure, including the vicinity of QDs [45,78], to be reduced, and hence, the observed recapturing processes and the occurrence of a slow decay component in the PL dynamics are suppressed.

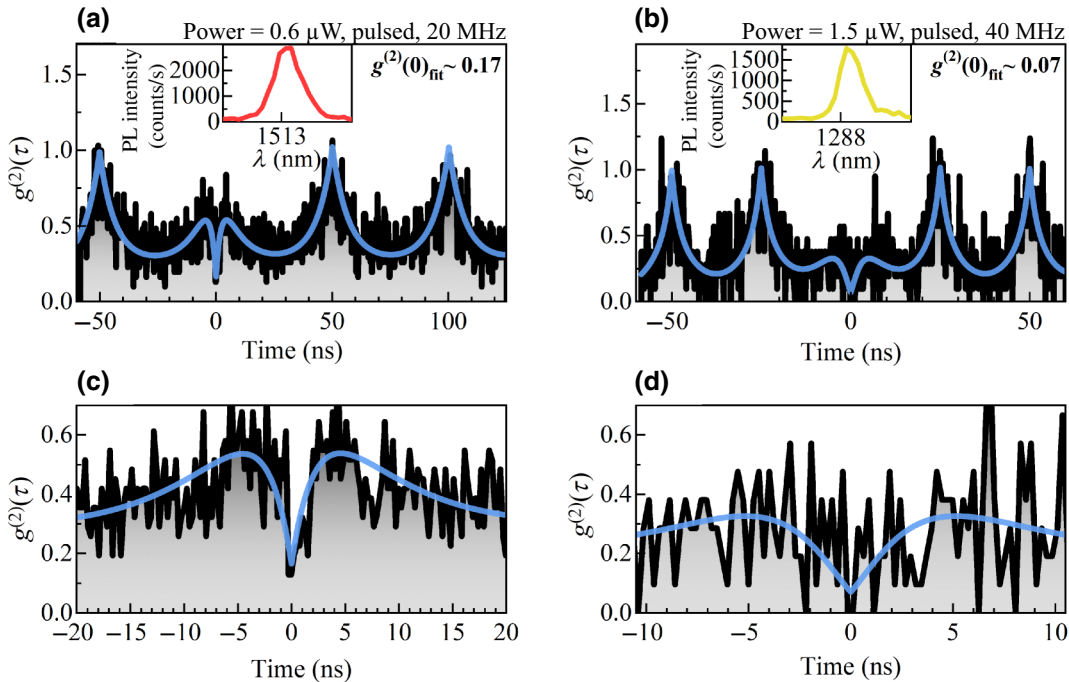


FIG. 9. Second-order correlation function, $g^{(2)}(\tau)$, for X emission under pulsed excitation with the 805-nm line (a) for structure In-38% and (b) for structure In-29%. Blue line is the fit to experimental data based on the additional recapture process and two-component decay, and insets show the emission spectra of the investigated lines. Magnified ranges for small delays for $g^{(2)}(\tau)$ dependence and fit (c) for the third telecom range and (d) for the second telecom range.

IV. CONCLUSION

We presented a study of single (In, Ga)As QDs that were grown by MBE on (In, Ga)As metamorphic buffers, on GaAs substrate. By changing the indium concentration in the top part of the MBL, we redshifted the QD emission and reached the third telecom window. We showed that the emission energy changed due to reduced strain in the QDs but also due to the varying indium content within the dots, which was induced by the composition changes in the MBL. We identified linewidths for many single QDs showing a slight increase for QDs on In-rich MBLs, suggesting a rise in the density of charge traps near QDs. In the polarization-resolved experiments, we obtained no fingerprint of the significant asymmetry change for different MBL compositions. The QD excited states could directly be probed in single dots by high-spatial-resolution photoluminescence excitation spectroscopy, allowing for the demonstration of the QD-emission linewidth decrease for quasiresonant excitation. We identified basic excitonic complexes and followed the changes in biexciton binding energy and fine-structure splitting for different MBL compositions, suggesting elongation of the dots emitting at longer wavelengths. The single-dot radiative lifetimes suggested a slight QD oscillator strength decrease for those on In-rich MBLs, whereas the ratios of the exciton-to-biexciton lifetimes and the slopes in the low-excitation-power dependences indicate an intermediate-confinement regime in these dots. We also demonstrated single-photon emission in the second and third telecom windows with $g^{(2)}(0)$ values comparable to those of InP-based QDs in the same range. This material system, grown by MBE, is relatively new compared to the more established MOVPE-grown solutions, but it already shows its competitiveness as a platform for telecom applications, also serving as a good alternative to InP-based QDs. Our results showed routes for further developments and optimizations, which should primarily concern improvements in the crystallographic quality of the MBL and reduction of the defect concentrations, which will affect many of the crucial properties, such as minimizing the contribution of the slow PL decay component or decreasing the inhomogenous linewidth, which, in turn, will improve the accuracy of FSS and $g^{(2)}(0)$ determination.

ACKNOWLEDGMENTS

We would like to thank Monika Emmerling (University of Würzburg) for the fabrication of mesas and apertures on the sample surface. We also thank Anna Musiał (Wrocław University of Science and Technology) for assistance with the optical spectroscopy setups. We are grateful to Krzysztof Gawarecki (Wrocław University of Science and Technology) for sharing his implementation of the $\mathbf{k}\cdot\mathbf{p}$ method. Numerical calculations were carried out using

resources provided by Wrocław Centre for Networking and Supercomputing [96]. P.A.W., F.J., and S.H. acknowledge financial support by the free state of Bavaria. S.H. and P.A.W. acknowledge financial support by the H2020 Marie Skłodowska-Curie Actions under ITN Project 4PHOTON (Grant Agreement No. 721394). P.W. acknowledges financial support by the European Union under the European Social Fund.

Conceptualization, P.P. and G.S.; methodology, P.W., M.G., P.P., M.P., and S.G.; investigation, P.W., M.G., M.P., and S.G.; formal analysis, P.W., M.G., P.P., and G.S.; funding acquisition, G.S. and S.H.; project administration, P.P. and G.S.; software, M.G.; writing – original draft preparation, P.W.; writing – review and editing, all authors; resources, P.A.W., F.J., and S.H.; supervision, P.P. and G.S.

The authors declare no conflict of interest.

-
- [1] C. Shang, Y. Wan, J. Selvidge, E. Hughes, R. Herrick, K. Mukherjee, J. Duan, F. Grillot, W. W. Chow, and J. E. Bowers, Perspectives on advances in quantum dot lasers and integration with Si photonic integrated circuits, *ACS Photonics* **8**, 2555 (2021).
 - [2] Z. Yao, C. Jiang, X. Wang, H. Chen, H. Wang, L. Qin, and Z. Zhang, Recent developments of quantum dot materials for high speed and ultrafast lasers, *Nanomaterials* **12**, 7 (2022).
 - [3] A. Yadav, N. B. Chichkov, E. A. Avrutin, A. Gorodetsky, and E. U. Rafailov, Edge emitting mode-locked quantum dot lasers, *Prog. Quantum Electron.* **87**, 100451 (2023).
 - [4] S. Bauer, V. Sichkovskyi, O. Eyal, T. Septon, A. Becker, I. Khanonkin, G. Eisenstein, and J. P. Reithmaier, 1.5- μ m indium phosphide-based quantum dot lasers and optical amplifiers: The impact of atom-like optical gain material for optoelectronics devices, *IEEE Nanotechnol. Mag.* **15**, 23 (2021).
 - [5] M. Z. M. Khan, T. K. Ng, and B. S. Ooi, Self-assembled InAs/InP quantum dots and quantum dashes: Material structures and devices, *Prog. Quantum Electron.* **38**, 237 (2014).
 - [6] N. Ozaki, K. Takeuchi, S. Ohkouchi, N. Ikeda, Y. Sugimoto, H. Oda, K. Asakawa, and R. A. Hogg, Monolithically grown multi-color InAs quantum dots as a spectral-shape-controllable near-infrared broadband light source, *Appl. Phys. Lett.* **103**, 051121 (2013).
 - [7] L. Seravalli, M. Gioannini, F. Cappelluti, F. Sacconi, G. Trevisi, and P. Frigeri, Broadband light sources based on InAs/InGaAs metamorphic quantum dots, *J. Appl. Phys.* **119**, 143102 (2016).
 - [8] P. Holewa, M. Gawełczyk, A. Maryński, P. Wyborski, J. P. Reithmaier, G. Sek, M. Benyoucef, and M. Syperek, Optical and electronic properties of symmetric InAs/(In, Al, Ga)As/InP quantum dots formed by ripening in molecular beam epitaxy: A potential system for broad-range single-photon telecom emitters, *Phys. Rev. Appl.* **14**, 064054 (2020).

- [9] S. Buckley, K. Rivoire, and J. Vučković, Engineered quantum dot single-photon sources, *Rep. Prog. Phys.* **75**, 126503 (2012).
- [10] P. Senellart, G. Solomon, and A. White, High-performance semiconductor quantum-dot single-photon sources, *Nat. Nanotechnol.* **12**, 11 (2017).
- [11] X. Cao, M. Zopf, and F. Ding, Telecom wavelength single photon sources, *J. Semicond.* **40**, 071901 (2019).
- [12] Y. Arakawa and M. J. Holmes, Progress in quantum-dot single photon sources for quantum information technologies: A broad spectrum overview, *Appl. Phys. Rev.* **7**, 021309 (2020).
- [13] C. Schimpf, M. Reindl, F. Basso Basset, K. D. Jöns, R. Trotta, and A. Rastelli, Quantum dots as potential sources of strongly entangled photons: Perspectives and challenges for applications in quantum networks, *Appl. Phys. Lett.* **118**, 100502 (2021).
- [14] S. Liu, K. Srinivasan, and J. Liu, Nanoscale positioning approaches for integrating single solid-state quantum emitters with photonic nanostructures, *Laser Photonics Rev.* **15**, 2100223 (2021).
- [15] A. Musiał, M. Mikulicz, P. Mrowiński, A. Zielińska, P. Sitarek, P. Wyborski, M. Kuniej, J. P. Reithmaier, G. Sek, and M. Benyoucef, InP-based single-photon sources operating at telecom C-band with increased extraction efficiency, *Appl. Phys. Lett.* **118**, 221101 (2021).
- [16] P. Holewa, A. Sakanas, U. M. Gür, P. Mrowiński, A. Huck, B.-Y. Wang, A. Musiał, K. Yvind, N. Gregersen, M. Syperek, and E. Semenova, Bright quantum dot single-photon emitters at telecom bands heterogeneously integrated on Si, *ACS Photonics* **9**, 2273 (2022).
- [17] F. Olbrich, J. Kettler, M. Bayerbach, M. Paul, J. Höschele, S. L. Portalupi, M. Jetter, and P. Michler, Temperature-dependent properties of single long-wavelength InGaAs quantum dots embedded in a strain reducing layer, *J. Appl. Phys.* **121**, 184302 (2017).
- [18] Ł Dusanowski, M. Syperek, J. Misiewicz, A. Somers, S. Höfling, M. Kamp, J. P. Reithmaier, and G. Sek, Single-photon emission of InAs/InP quantum dashes at 1.55 μm and temperatures up to 80 K, *Appl. Phys. Lett.* **108**, 163108 (2016).
- [19] A. W. Elshaari, W. Pernice, K. Srinivasan, O. Benson, and V. Zwiller, Hybrid integrated quantum photonic circuits, *Nat. Photonics* **14**, 5 (2020).
- [20] S. L. Portalupi, M. Jetter, and P. Michler, InAs quantum dots grown on metamorphic buffers as non-classical light sources at telecom C-band: A review, *Semicond. Sci. Technol.* **34**, 053001 (2019).
- [21] P. Holewa, S. Kadkhodazadeh, M. Gawełczyk, P. Baluta, A. Musiał, V. G. Dubrovskii, M. Syperek, and E. Semenova, Droplet epitaxy symmetric InAs/InP quantum dots for quantum emission in the third telecom window: Morphology, optical and electronic properties, *Nanophotonics* **11**, 1515 (2022).
- [22] A. Barbiero, J. Huwer, J. Skiba-Szymanska, D. J. P. Ellis, R. M. Stevenson, T. Müller, G. Shooter, L. E. Goff, D. A. Ritchie, and A. J. Shields, High-performance single-photon sources at telecom wavelength based on broadband hybrid circular Bragg gratings, *ACS Photonics* **9**, 3060 (2022).
- [23] M. D. Birowosuto, H. Sumikura, S. Matsuo, H. Taniyama, P. J. van Veldhoven, R. Nötzel, and M. Notomi, Fast Purcell-enhanced single photon source in 1.550-μm telecom band from a resonant quantum dot-cavity coupling, *Sci. Rep.* **2**, 1 (2012).
- [24] X. Liu, K. Akahane, N. A. Jahan, N. Kobayashi, M. Sasaki, H. Kumano, and I. Suemune, Single-photon emission in telecommunication band from an InAs quantum dot grown on InP with molecular-beam epitaxy, *Appl. Phys. Lett.* **103**, 061114 (2013).
- [25] Ł Dusanowski, M. Syperek, P. Mrowiński, W. Rudno-Rudziński, J. Misiewicz, A. Somers, S. Höfling, M. Kamp, J. P. Reithmaier, and G. Sek, Single photon emission at 1.55 μm from charged and neutral exciton confined in a single quantum dash, *Appl. Phys. Lett.* **105**, 021909 (2014).
- [26] K. Takemoto, Y. Nambu, T. Miyazawa, Y. Sakuma, T. Yamamoto, S. Yorozu, and Y. Arakawa, Quantum key distribution over 120 km using ultrahigh purity single-photon source and superconducting single-photon detectors, *Sci. Rep.* **5**, 1 (2015).
- [27] T. Müller, J. Skiba-Szymanska, A. B. Krysa, J. Huwer, M. Felle, M. Anderson, R. M. Stevenson, J. Heffernan, D. A. Ritchie, and A. J. Shields, A quantum light-emitting diode for the standard telecom window around 1,550 μm, *Nat. Commun.* **9**, 1 (2018).
- [28] P. Wyborski, A. Musiał, P. Mrowiński, P. Podemski, V. Baumann, P. Wroński, F. Jabeen, S. Höfling, and G. Sek, InP-substrate-based quantum dashes on a DBR as single-photon emitters at the third telecommunication window, *Materials* **14**, 4 (2021).
- [29] M. Anderson, T. Müller, J. Huwer, J. Skiba-Szymanska, A. B. Krysa, R. M. Stevenson, J. Heffernan, D. A. Ritchie, and A. J. Shields, Quantum teleportation using highly coherent emission from telecom C-band quantum dots, *Npj Quantum Inf.* **6**, 1 (2020).
- [30] M. Anderson, T. Müller, J. Skiba-Szymanska, A. B. Krysa, J. Huwer, R. M. Stevenson, J. Heffernan, D. A. Ritchie, and A. J. Shields, Coherence in single photon emission from droplet epitaxy and Stranski-Krastanov quantum dots in the telecom C-band, *Appl. Phys. Lett.* **118**, 014003 (2021).
- [31] L. Wells, T. Müller, R. M. Stevenson, J. Skiba-Szymanska, D. A. Ritchie, and A. J. Shields, Coherent Light Scattering from a Telecom C-Band Quantum Dot, [arXiv:2205.07997](https://arxiv.org/abs/2205.07997).
- [32] G. Shooter, Z.-H. Xiang, J. R. A. Müller, J. Skiba-Szymanska, J. Huwer, J. Griffiths, T. Mitchell, M. Anderson, T. Müller, A. B. Krysa, *et al.*, 1 GHz clocked distribution of electrically generated entangled photon pairs, *Opt. Express* **28**, 36838 (2020).
- [33] M. Anderson, T. Müller, J. Skiba-Szymanska, A. B. Krysa, J. Huwer, R. M. Stevenson, J. Heffernan, D. A. Ritchie, and A. J. Shields, Gigahertz-paced teleportation of time-bin qubits with a quantum dot in the telecommunication C band, *Phys. Rev. Appl.* **13**, 054052 (2020).
- [34] L. Seravalli, M. Minelli, P. Frigeri, P. Allegri, V. Avanzini, and S. Franchi, The effect of strain on tuning of light emission energy of InAs/InGaAs quantum-dot nanostructures, *Appl. Phys. Lett.* **82**, 2341 (2003).
- [35] A. R. Kovsh, A. E. Zhukov, N. A. Maleev, S. S. Mikhlin, V. M. Ustinov, A. F. Tsatsul'nikov, M. V. Maksimov, B. V.

- Volovik, D. A. Bedarev, Yu. M. Shernyakov, *et al.*, Lasing at a wavelength close to 1.3 μm in InAs quantum-dot structures, *Semiconductors* **33**, 929 (1999).
- [36] R. Heitz, I. Mukhametzhanov, A. Madhukar, A. Hoffmann, and D. Bimberg, Temperature dependent optical properties of self-organized InAs/GaAs quantum dots, *J. Electron. Mater.* **28**, 520 (1999).
- [37] C. Carmesin, F. Olbrich, T. Mehrtens, M. Florian, S. Michael, S. Schreier, C. Nawrath, M. Paul, J. Höschele, B. Gerken, *et al.*, Structural and optical properties of InAs/(In)GaAs/GaAs quantum dots with single-photon emission in the telecom C-band up to 77 K, *Phys. Rev. B* **98**, 125407 (2018).
- [38] L. H. Li, M. Rossetti, G. Patriarche, and A. Fiore, Growth of InAs bilayer quantum dots for long-wavelength laser emission on GaAs, *J. Cryst. Growth* **301–302**, 959 (2007).
- [39] B. Alloing, C. Zinoni, L. H. Li, A. Fiore, and G. Patriarche, Structural and optical properties of low-density and In-rich InAs/GaAs quantum dots, *J. Appl. Phys.* **101**, 024918 (2007).
- [40] P. Wyborski, P. Podemski, P. A. Wroński, F. Jabeen, S. Höfling, and G. Sek, Electronic and optical properties of InAs QDs grown by MBE on InGaAs metamorphic buffer, *Materials* **15**, 3 (2022).
- [41] M. Paul, F. Olbrich, J. Höschele, S. Schreier, J. Kettler, S. L. Portalupi, M. Jetter, and P. Michler, Single-photon emission at 1.55 μm from MOVPE-grown InAs quantum dots on InGaAs/GaAs metamorphic buffers, *Appl. Phys. Lett.* **111**, 033102 (2017).
- [42] E. S. Semenova, A. E. Zhukov, S. S. Mikhrin, A. Y. Egorov, V. A. Odnoblyudov, A. P. Vasil'ev, E. V. Nikitina, A. R. Kovsh, N. V. Kryzhanovskaya, A. G. Gladyshev, *et al.*, Metamorphic growth for application in long-wavelength (1.3–1.55 μm) lasers and MODFET-type structures on GaAs substrates, *Nanotechnology* **15**, S283 (2004).
- [43] E. S. Semenova, R. Hostein, G. Patriarche, O. Mauguin, L. Largeau, I. Robert-Philip, A. Beveratos, and A. Lemaitre, Metamorphic approach to single quantum dot emission at 1.55 μm on GaAs substrate, *J. Appl. Phys.* **103**, 103533 (2008).
- [44] L. Seravalli, P. Frigeri, G. Trevisi, and S. Franchi, 1.59 μm room temperature emission from metamorphic InAs/InGaAs quantum dots grown on GaAs substrates, *Appl. Phys. Lett.* **92**, 213104 (2008).
- [45] B. Scaparra, A. Ajay, P. S. Avdienko, Y. Xue, H. Ried, P. Kohl, B. Jonas, B. Costa, E. Sirotti, P. Schmiedeke, *et al.*, Structural properties of graded In_xGa_{1-x}As metamorphic buffer layers for quantum dots emitting in the telecom bands, *Mater. Quantum Technol.* **3**, 035004 (2023).
- [46] P. A. Wroński, P. Wyborski, A. Musiał, P. Podemski, G. Sek, S. Höfling, and F. Jabeen, Metamorphic buffer layer platform for 1550 nm single-photon sources grown by MBE on (100) GaAs substrate, *Materials* **14**, 18 (2021).
- [47] R. Sittig, C. Nawrath, S. Kolatschek, S. Bauer, R. Schaber, J. Huang, P. Vijayan, P. Pruy, S. L. Portalupi, M. Jetter, and P. Michler, Thin-film InGaAs metamorphic buffer for telecom C-band InAs quantum dots and optical resonators on GaAs platform, *Nanophotonics* **11**, 1109 (2022).
- [48] N. A. Maleev, A. V. Sakharov, C. Moeller, I. L. Krestnikov, A. R. Kovsh, S. S. Mikhrin, A. E. Zhukov, V. M. Ustinov, W. Passenberg, E. Pawłowski, *et al.*, 1300 nm GaAs-based microcavity LED incorporating InAs/GaInAs quantum dots, *J. Cryst. Growth* **227–228**, 1146 (2001).
- [49] F. Olbrich, J. Hoeschele, M. Mueller, J. Kettler, S. L. Portalupi, M. Paul, M. Jetter, and P. Michler, Polarization-entangled photons from an InGaAs-based quantum dot emitting in the telecom C-band, *Appl. Phys. Lett.* **111**, 133106 (2017).
- [50] K. D. Zeuner, K. D. Jöns, L. Schweickert, C. R. Hedlund, C. Nuñez Lobato, T. Lettner, K. Wang, S. Gyger, E. Schöll, S. Steinhauer, *et al.*, On-demand generation of entangled photon pairs in the telecom C-band with InAs quantum dots, *ACS Photonics* **8**, 2337 (2021).
- [51] C. Nawrath, F. Olbrich, M. Paul, S. L. Portalupi, M. Jetter, and P. Michler, Coherence and indistinguishability of highly pure single photons from non-resonantly and resonantly excited telecom C-band quantum dots, *Appl. Phys. Lett.* **115**, 023103 (2019).
- [52] C. Nawrath, H. Vural, J. Fischer, R. Schaber, S. L. Portalupi, M. Jetter, and P. Michler, Resonance fluorescence of single In(Ga)As quantum dots emitting in the telecom C-band, *Appl. Phys. Lett.* **118**, 244002 (2021).
- [53] C. Nawrath, R. Joos, S. Kolatschek, S. Bauer, P. Pruy, F. Hornung, J. Fischer, J. Huang, P. Vijayan, R. Sittig, *et al.*, Bright source of Purcell-enhanced, triggered, single photons in the telecom C-band, *Adv. Quantum Technol.* **1**, 2300111 (2023).
- [54] K. D. Zeuner, M. Paul, T. Lettner, C. Reuterskiöld Hedlund, L. Schweickert, S. Steinhauer, L. Yang, J. Zichi, M. Hammar, K. D. Jöns, and V. Zwiller, A stable wavelength-tunable triggered source of single photons and cascaded photon pairs at the telecom C-band, *Appl. Phys. Lett.* **112**, 173102 (2018).
- [55] T. Lettner, S. Gyger, K. D. Zeuner, L. Schweickert, S. Steinhauer, C. Reuterskiöld Hedlund, Sandra Stroj, Armando Rastelli, Mattias Hammar, Rinaldo Trotta, *et al.*, Strain-controlled quantum dot fine structure for entangled photon generation at 1550 μm , *Nano Lett.* **21**, 10501 (2021).
- [56] Ł. Dusanowski, C. Nawrath, S. L. Portalupi, M. Jetter, T. Huber, S. Klembt, P. Michler, and S. Höfling, Optical charge injection and coherent control of a quantum-dot spin-qubit emitting at telecom wavelengths, *Nat. Commun.* **13**, 1 (2022).
- [57] N. N. Ledentsov, A. R. Kovsh, A. E. Zhukov, N. A. Maleev, S. S. Mikhrin, A. P. Vasil'ev, E. S. Semenova, M. V. Maximov, Y. M. Shemyakov, N. V. Kryzhanovskaya, *et al.*, High performance quantum dot lasers on GaAs substrates operating in 1.5 μm range, *Electron. Lett.* **39**, 1126 (2003).
- [58] L. Seravalli, G. Trevisi, G. Muñoz-Matutano, D. Rivas, J. Martínez-Pastor, and P. Frigeri, Sub-critical InAs layers on metamorphic InGaAs for single quantum dot emission at telecom wavelengths, *Cryst. Res. Technol.* **49**, 540 (2014).
- [59] P. Podemski, A. Maryński, P. Wyborski, A. Bercha, W. Trzeciakowski, and G. Sek, Single dot photoluminescence excitation spectroscopy in the telecommunication spectral range, *J. Lumin.* **212**, 300 (2019).
- [60] K. Gawarecki, P. Machnikowski, and T. Kuhn, Electron states in a double quantum dot with broken axial symmetry, *Phys. Rev. B* **90**, 085437 (2014).
- [61] T. B. Bahder, Eight-band $\mathbf{k}\cdot\mathbf{p}$ model of strained zinc-blende crystals, *Phys. Rev. B* **41**, 11992 (1990).

- [62] A. Miernik-Pyszczorski, K. Gawarecki, M. Gawełczyk, and P. Machnikowski, Dominant role of the shear strain induced admixture in spin-flip processes in self-assembled quantum dots, *Phys. Rev. B* **97**, 245313 (2018).
- [63] M. Gawełczyk, M. Syperek, A. Maryński, P. Mrowiński, Ł Dusanowski, K. Gawarecki, J. Misiewicz, A. Somers, J. P. Reithmaier, S. Höfling, and G. Sek, Exciton lifetime and emission polarization dispersion in strongly in-plane asymmetric nanostructures, *Phys. Rev. B* **96**, 245425 (2017).
- [64] A. Thränhardt, C. Ell, G. Khitrova, and H. M. Gibbs, Relation between dipole moment and radiative lifetime in interface fluctuation quantum dots, *Phys. Rev. B* **65**, 035327 (2002).
- [65] J. Andrzejewski, G. Sek, E. O'Reilly, A. Fiore, and J. Misiewicz, Eight-band $\mathbf{k}\cdot\mathbf{p}$ calculations of the composition contrast effect on the linear polarization properties of columnar quantum dots, *J. Appl. Phys.* **107**, 073509 (2010).
- [66] J. M. Ulloa, C. Çelebi, P. M. Koenraad, A. Simon, E. Gapihan, A. Letoublon, N. Bertru, I. Drouzas, D. J. Mowbray, M. J. Steer, and M. Hopkinson, Atomic scale study of the impact of the strain and composition of the capping layer on the formation of InAs quantum dots, *J. Appl. Phys.* **101**, 081707 (2007).
- [67] V. M. Ustinov, N. A. Maleev, A. E. Zhukov, A. R. Kovsh, A. Yu. Egorov, A. V. Lunev, B. V. Volovik, I. L. Krestnikov, Yu. G. Musikhin, N. A. Bert, *et al.*, InAs/InGaAs quantum dot structures on GaAs substrates emitting at 1.3 μm, *Appl. Phys. Lett.* **74**, 2815 (1999).
- [68] A. Fiore, U. Oesterle, R. P. Stanley, R. Houdré, F. Lelarge, M. Illegems, P. Borri, W. Langbein, D. Birkedal, J. M. Hvam, *et al.*, Structural and electrooptical characteristics of quantum dots emitting at 1.3 μm on gallium arsenide, *IEEE J. Quantum Electron.* **37**, 1050 (2001).
- [69] L. Seravalli, P. Frigeri, L. Nasi, G. Trevisi, and C. Bocchi, Metamorphic quantum dots: Quite different nanostructures, *J. Appl. Phys.* **108**, 064324 (2010).
- [70] E. F. Schubert, E. O. Göbel, Y. Horikoshi, K. Ploog, and H. J. Queisser, Alloy broadening in photoluminescence spectra of $\text{Al}_x\text{Ga}_{1-x}\text{As}$, *Phys. Rev. B* **30**, 813 (1984).
- [71] Ł Dusanowski, A. Musiał, A. Maryński, P. Mrowiński, J. Andrzejewski, P. Machnikowski, J. Misiewicz, A. Somers, S. Höfling, J. P. Reithmaier, and G. Sek, Phonon-assisted radiative recombination of excitons confined in strongly anisotropic nanostructures, *Phys. Rev. B* **90**, 125424 (2014).
- [72] A. Musiał, G. Sek, P. Podemski, M. Syperek, J. Misiewicz, A. Löffler, S. Höfling, and A. Forchel, Excitonic complexes in InGaAs/GaAs quantum dash structures, *J. Phys.: Conf. Ser.* **245**, 012054 (2010).
- [73] Ł Dusanowski, M. Syperek, A. Maryński, L. H. Li, J. Misiewicz, S. Höfling, M. Kamp, A. Fiore, and G. Sek, Single photon emission up to liquid nitrogen temperature from charged excitons confined in GaAs-based epitaxial nanostructures, *Appl. Phys. Lett.* **106**, 233107 (2015).
- [74] M. Abbarchi, F. Troiani, C. Mastrandrea, G. Goldoni, T. Kuroda, T. Mano, K. Sakoda, N. Koguchi, S. Sanguineti, A. Vinattieri, and M. Gurioli, Spectral diffusion and line broadening in single self-assembled GaAs/AlGaAs quantum dot photoluminescence, *Appl. Phys. Lett.* **93**, 162101 (2008).
- [75] M. Bayer, G. Ortner, O. Stern, A. Kuther, A. A. Gorbunov, A. Forchel, P. Hawrylak, S. Fafard, K. Hinzer, T. L. Reinecke, *et al.*, Fine structure of neutral and charged excitons in self-assembled In(Ga)As/(Al)GaAs quantum dots, *Phys. Rev. B* **65**, 195315 (2002).
- [76] C. Zinoni, B. Alloing, C. Monat, V. Zwiller, L. H. Li, A. Fiore, L. Lunghi, A. Gerardino, H. de Riedmatten, H. Zbinden, and N. Gisin, Time-resolved and antibunching experiments on single quantum dots at 1300 nm, *Appl. Phys. Lett.* **88**, 86 (2006).
- [77] M. Gschrey, F. Gericke, A. Schüßler, R. Schmidt, J. H. Schulze, T. Heindel, S. Rodt, A. Strittmatter, and S. Reitzenstein, *In situ* electron-beam lithography of deterministic single-quantum-dot mesa-structures using low-temperature cathodoluminescence spectroscopy, *Appl. Phys. Lett.* **102**, 251113 (2013).
- [78] S. V. Sorokin, G. V. Klimko, I. V. Sedova, A. A. Sitnikova, D. A. Kirilenko, M. V. Baidakova, M. A. Yagovkina, T. A. Komissarova, K. G. Belyaev, and S. V. Ivanov, Peculiarities of strain relaxation in linearly graded $\text{In}_x\text{Ga}_{1-x}\text{As}/\text{GaAs}(001)$ metamorphic buffer layers grown by molecular beam epitaxy, *J. Cryst. Growth* **455**, 83 (2016).
- [79] C. Tonin, R. Hostein, V. Voliotis, R. Grousson, A. Lemaitre, and A. Martinez, Polarization properties of excitonic qubits in single self-assembled quantum dots, *Phys. Rev. B* **85**, 155303 (2012).
- [80] J. P. Reithmaier, A. Somers, S. Deubert, R. Schwertberger, W. Kaiser, A. Forchel, M. Calligaro, P. Resneau, O. Parillaud, S. Bansropun, *et al.*, InP based lasers and optical amplifiers with wire-/dot-like active regions, *J. Phys. D: Appl. Phys.* **38**, 2088 (2005).
- [81] A. Löffler, J.-P. Reithmaier, A. Forchel, A. Sauerwald, D. Peskes, T. Kümmell, and G. Bacher, Influence of the strain on the formation of GaInAs/GaAs quantum structures, *J. Cryst. Growth* **286**, 6 (2006).
- [82] A. Musiał, P. Podemski, G. Sek, P. Kaczmarkiewicz, J. Andrzejewski, P. Machnikowski, J. Misiewicz, S. Hein, A. Somers, S. Höfling, *et al.*, Height-driven linear polarization of the surface emission from quantum dashes, *Semicond. Sci. Technol.* **27**, 105022 (2012).
- [83] Y. Léger, L. Besombes, L. Maingault, and H. Mariette, Valence-band mixing in neutral, charged, and Mn-doped self-assembled quantum dots, *Phys. Rev. B* **76**, 045331 (2007).
- [84] A. V. Koudinov, I. A. Akimov, Yu. G. Kusrayev, and F. Henneberger, Optical and magnetic anisotropies of the hole states in Stranski-Krastanov quantum dots, *Phys. Rev. B* **70**, 241305 (2004).
- [85] G. Sek, A. Musiał, P. Podemski, and J. Misiewicz, On the applicability of a few level rate equation model to the determination of exciton versus biexciton kinetics in quasi-zero-dimensional structures, *J. Appl. Phys.* **108**, 033507 (2010).
- [86] Ł Dusanowski, M. Syperek, W. Rudno-Rudziński, P. Mrowiński, G. Sek, J. Misiewicz, A. Somers, J. P. Reithmaier, S. Höfling, and A. Forchel, Exciton and biexciton dynamics in single self-assembled InAs/InGaAlAs/InP quantum dash emitting near 1.55 μm, *Appl. Phys. Lett.* **103**, 253113 (2013).
- [87] S. Rodt, R. Seguin, A. Schliwa, F. Guffarth, K. Pötschke, U. W. Pohl, and D. Bimberg, Size-dependent binding energies

- and fine-structure splitting of excitonic complexes in single InAs/GaAs quantum dots, *J. Lumin.* **122–123**, 735 (2007).
- [88] G. Sęk, P. Podemski, J. Misiewicz, L. H. Li, A. Fiore, and G. Patriarche, Photoluminescence from a single InGaAs epitaxial quantum rod, *Appl. Phys. Lett.* **92**, 021901 (2008).
- [89] L. Seravalli, G. Trevisi, P. Frigeri, D. Rivas, G. Muñoz-Matutano, I. Suárez, B. Alén, J. Canet-Ferrer, and J. P. Martínez-Pastor, Single quantum dot emission at telecom wavelengths from metamorphic InAs/InGaAs nanostructures grown on GaAs substrates, *Appl. Phys. Lett.* **98**, 173112 (2011).
- [90] K. Takemoto, M. Takatsu, S. Hirose, N. Yokoyama, Y. Sakuma, T. Usuki, T. Miyazawa, and Y. Arakawa, An optical horn structure for single-photon source using quantum dots at telecommunication wavelength, *J. Appl. Phys.* **101**, 081720 (2007).
- [91] A. Musiał, P. Holewa, P. Wyborski, M. Syperek, A. Kors, J. P. Reithmaier, G. Sęk, and M. Benyoucef, High-purity triggered single-photon emission from symmetric single InAs/InP quantum dots around the telecom C-band window, *Adv. Quantum Technol.* **3**, 1900082 (2020).
- [92] N. Ha, T. Mano, S. Dubos, T. Kuroda, Y. Sakuma, and K. Sakoda, Single photon emission from droplet epitaxial quantum dots in the standard telecom window around a wavelength of 1.55 μm, *Appl. Phys. Express* **13**, 025002 (2020).
- [93] P. A. Dalgarno, J. McFarlane, D. Brunner, R. W. Lambert, B. D. Gerardot, R. J. Warburton, K. Karrai, A. Badolato, and P. M. Petroff, Hole recapture limited single photon generation from a single *n*-type charge-tunable quantum dot, *Appl. Phys. Lett.* **92**, 193103 (2008).
- [94] S. Fischbach, A. Schleehahn, A. Thoma, N. Srocka, T. Gissibl, S. Ristok, S. Thiele, A. Kaganskiy, A. Strittmatter, T. Heindel, *et al.*, Single quantum dot with microlens and 3D-printed micro-objective as integrated bright single-photon source, *ACS Photonics* **4**, 1327 (2017).
- [95] T. Miyazawa, K. Takemoto, Y. Nambu, S. Miki, T. Yamashita, H. Terai, M. Fujiwara, M. Sasaki, Y. Sakuma, M. Takatsu, *et al.*, Single-photon emission at 1.5 μm from an InAs/InP quantum dot with highly suppressed multi-photon emission probabilities, *Appl. Phys. Lett.* **109**, 132106 (2016).
- [96] <https://wcss.pl>.